



Phase-sensitive manipulation of squeezed vacuum via a dual-recycled Michelson interferometer

WEI LI,^{1,2}  YAOHUA PENG,² XUDONG YU,^{1,3}  LIRONG CHEN,² AND YAOHUI ZHENG^{1,3,*} 

¹State Key Laboratory of Quantum Optics and Quantum Optics Devices, Institute of Opto-Electronics, Shanxi University, Taiyuan 030006, China

²College of Physics and Electronic Engineering, Shanxi University, Taiyuan, Shanxi 030006, China

³Collaborative Innovation Center of Extreme Optics, Shanxi University, Taiyuan, Shanxi 030006, China
*yhzeng@sxu.edu.cn

Abstract: The injection of squeezed vacuum state is an indispensable technology for the next generation gravitational wave observatory, which will open up a much larger window to the universe. After analyzing the absorption and dispersion properties of the reflected field of the dual-recycled Michelson interferometer (DRMI), we propose the phase-sensitive manipulation scheme of squeezed vacuum by utilizing the coupled-resonator-induced transparency in a dual-recycled Michelson interferometer (DRMI). In this way, the rotation frequency of squeezing ellipse can be finely tuned by the coupling strength, which overcome the limitation of the current solution (with a fixed rotation frequency) that employs a Fabry-Perot optical cavity as phase-sensitive manipulation element. This work will unleash the potential applications for quantum metrology beyond the shot noise limit.

© 2021 Optical Society of America under the terms of the [OSA Open Access Publishing Agreement](#)

1. Introduction

Gravitational waves (GWs) are ripples in spacetime generated by massive accelerating objects, as predicted by Albert Einstein in his general relativity. In 2015, the first direct detection of GWs emitted by a binary black hole merger [1] was announced by the Laser Interferometer Gravitational-wave Observatory (LIGO), which was also the dawn of gravitational wave astronomy. Since then, over fifty binary black hole mergers [2–6] and a neutron star merger [7] were detected by the National Science Foundation's LIGO and the European Union's Virgo. In 2020, two elusive mergers of black holes with neutron stars were observed successively by LIGO and Virgo scientific collaborations [8].

The direct detection of GWs is achieved by the dual-recycled Fabry-Perot Michelson interferometer (DRFPMI) [9] that consists of a power recycling mirror, a signal recycling mirror, a traditional Michelson interferometer (MI) and Fabry-Perot cavities in both arms. The MI is operated such that laser from two orthogonal arms interfere destructively at the 50/50 beam splitter (HBS) in the absence of GWs. When the GWs arrive, the distances of two perpendicular arms are affected in opposite ways, for example, the distances increase along x direction while decrease along y direction. With a kilometer-scale arm length, the operational gravitational wave detectors (GWD) can reach the strain sensitivity of $10^{-23}/\sqrt{\text{Hz}}$ [10,11]. The additional power recycling resonator increases the power in each perpendicular arm and thus amplifies the sensitivity of GWD, while the signal recycling resonator tunes the measurement bandwidth [12].

In order to build a "third generation" (3G) gravitational wave observatory whose sensitivity is ten times larger than that of Advanced LIGO, the injection of squeezed vacuum state is an indispensable technology [13]. Squeezed state is a nonclassical state whose quantum fluctuations in one quadrature is less than vacuum noise at the cost of increased fluctuations in orthogonal

quadrature. Since the first experimental generation in 1985 [14], the squeezed state has exhibited an unpredictable prospect in quantum communication [15,16], quantum network [17] and quantum metrology [18]. The squeezing-enhanced technique (SET) was first proposed in 1981 [19] and has subsequently been demonstrated in prototype interferometer [20,21]. The GEO600 detector in Germany has introduced squeezing technique since 2010 and improved sensitivity at above 700 Hz [22]. In 2013, the SET was applied to large-scale interferometer (LIGO), and the maximum improvement to the sensitivity was 2.3 dB [23]. In 2019, the sensitivity improvement of Advanced LIGO detectors was up to 3 dB at high frequency by employing a frequency-independent squeezing [24], thereby increasing the detection rate by 40% (H1) and 50% (L1). More specifically, there are two kinds of quantum noise that limits the sensitivity of GWD. The shot noise at high frequency is introduced by phase fluctuations of optical field, whereas the radiation pressure noise at low frequency is introduced by amplitude fluctuations. Because of the amplified quantum fluctuation of orthogonal quadrature, the traditional SET can not reduce the quantum noise of GWD in whole frequency band [25,26].

For broadband quantum noise reduction of GWD, the frequency-dependent squeezing, whose angle of squeezing ellipse rotates by 90° around corner frequency [27,28] that depends on the laser power and interferometer parameters, is essential. The frequency-dependent squeezing is produced by phase-sensitive manipulation of squeezed vacuum from a filter cavity, which is proposed by H. J. Kimble [29]. Subsequently, the frequency-dependent squeezing around several discrete frequencies [30–32] are generated by employing an additional filter cavity, respectively, the rotational frequency is determined by the linewidth of filter cavity [33]. However, the linewidth of filter cavity is generally constant, which imposes restrictions on the tunability of the rotation frequency, it is unacceptable to meet the requirement for universality.

The phase-sensitive manipulation of squeezed vacuum has been demonstrated in coupled standing-wave cavities, but the coupling strength is constant, not be tuned [34]. In this letter, we propose the phase-sensitive manipulation scheme of squeezed vacuum in virtue of the coupled-resonator-induced transparency (CRIT) in DRMI. By formulating the reflective quantum fluctuation spectra of DRMI, we exhibit that the rotation frequency of squeezing ellipse can be finely tuned by the coupling strength that is manipulated by adjusting the relative phase difference between two interferometer arms [35]. This work will unleash the potential applications for quantum metrology beyond the shot noise limit.

2. Classical characteristic of DRMI

The schematic diagram of dual-recycled Michelson interferometer is sketched in Fig. 1(a). An input laser is divided into two perpendicular beams by a balanced beam splitter (BBS) and reflected back by two highly reflective mirrors (M_{a1} and M_{a2}). The arm length, which is kilometer scale for the operational ground-based gravitation wave detectors, is defined as the distance between BBS and highly reflective mirror. Two additional mirrors M_2 and M_0 constitute the so-called power recycling resonator and signal recycling resonator respectively. For briefness, the optical lengths between BBS and four reflective mirrors are assumed to be identical, which can be finely tuned by the piezoelectric transducers (PZT) mounted behind the mirrors.

As shown inside the dash box of Fig. 1(b), the BBS, two highly reflective mirrors (M_{a1} and M_{a2}) and the signal recycling mirror M_0 are equivalent to a single optical cavity (SOC1). Based on the input and output equation of the electromagnetic field, the reflected coefficient of SOC1 can be formulated as

$$\gamma_1 = e^{i(\theta_{a2} + \theta_{a1})} \frac{r_1 + r_0 e^{i(2\theta_0 + \theta_{a2} + \theta_{a1})}}{1 + r_1 r_0 e^{i(2\theta_0 + \theta_{a2} + \theta_{a1})}} \quad (1)$$

where $\theta_j = 2\pi(\omega_0 + \omega)T_j$ ($j = a_1, a_2, 0$) is the single-pass phase shift of each subcavity, and $T_j = l_j/c$ is the single-pass time (we set $T_j = T$ on account of the identical optical length $l_j = l$). ω_0 and ω are the resonant and detuning frequency respectively, and c is the speed of light. The

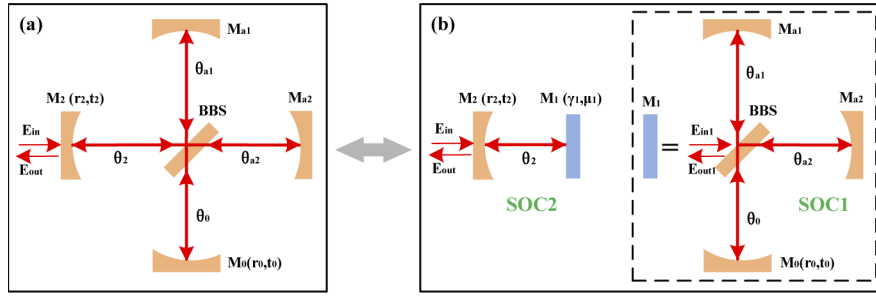


Fig. 1. (a) Schematic diagram of dual-recycled Michelson interferometer. M_{a1} and M_{a2} are the highly reflective mirrors for two interferometer arms. M_2 and M_0 are the power recycling mirror and signal recycling mirror respectively. (b) The equivalent single optical cavity (SOC2) that consist of a power recycling mirror M_2 and a mirror M_1 with variational reflectivity. BBS: balanced beam splitter.

reflectivity of M_{a1} and M_{a2} is fixed to be one for simplicity, while the reflectivity of M_0 is r_0 . An extra phase $e^{i(\theta_{a2} + \theta_{a1})}$ is introduced by two interferometer arms l_{a2} and l_{a1} . Compared with the traditional coupled resonator, the BBS, M_{a1} and M_{a2} can be regarded as a middle mirror with controllable reflectivity $r_1 = \cos(\Delta\theta)$, where $\Delta\theta = \theta_{a1} - \theta_{a2}$. Thus the coupling strength $\Omega = \frac{c}{4l} \sqrt{1 - r_1^2}$ can be controlled fleetly by the relative phase between two perpendicular interferometer arms.

Suppose the equivalent cavity is a mirror $M_1(\gamma_1, \mu_1)$ with variational reflectivity γ_1 , the dual-recycled Michelson interferometer can be considered as another single optical cavity (SOC2) that is composed of power recycling mirror M_2 and equivalent mirror M_1 . Therefore the reflected coefficient of dual-recycled Michelson interferometer can be expressed as

$$\gamma_2 = \frac{r_2 + \gamma_1 e^{2i\theta_2}}{1 + r_2 \gamma_1 e^{2i\theta_2}} \quad (2)$$

where r_2 is the reflectivity of power recycling mirror M_2 , and $\theta_2 = 2\pi(\omega_0 + \omega)T_2$ is the single-pass phase shift of equivalent single optical cavity (SOC2).

Hence the amplitude and phase shift of the reflected field of the dual-recycled Michelson interferometer can be described as

$$\begin{aligned} \rho &= Abs(\gamma_2) \\ \theta &= Arg(\gamma_2) \end{aligned}$$

Figure 2 represent the absorption and dispersion properties of dual-recycled Michelson interferometer with different coupling strength. In Fig. 2(a)-(f), the relative phase difference between two interference arms θ_{a1} and θ_{a2} are 0.001π , 0.006π , 0.014π , 0.02π , 0.08π , 0.12π in turn, corresponding to the coupling strength $\Omega = 2\pi * 1.3$ MHz, $2\pi * 8.0$ MHz, $2\pi * 18.6$ MHz, $2\pi * 26.6$ MHz, $2\pi * 105.3$ MHz, $2\pi * 155.8$ MHz respectively. In the weak coupling strength region (Fig. 2(a)), the impedance matching and thus the transmissivity of DRMI will increase with the increased coupling strength. In the strong coupling strength region (Fig. 2(b) - (e)), the reflected amplitude of DRMI will split and exhibit a coupled-resonator-induced transparent window, whose width can be controlled by adjusting the coupling strength (or the arm lengths). Continue to increase the coupling strength, the single resonant peak of DRMI will separate into two independent resonant peaks (Fig. 2(f)).

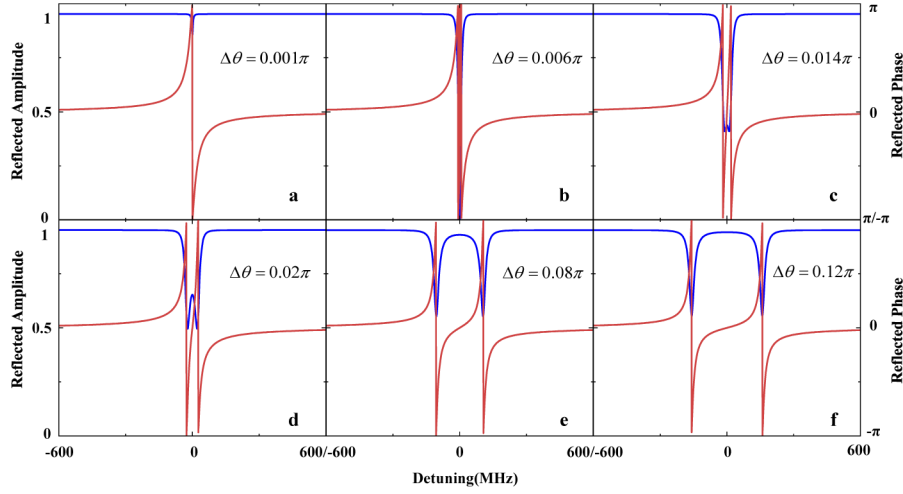


Fig. 2. Power reflectivity (blue curve) and phase shift (red curve) of dual-recycled Michelson interferometer. The single-pass phases $\theta_0 = \theta_2 = 2n\pi + \omega T$ ($n = 1, 2, \dots$), where ωT is the phase shift caused by the detuning away from the cavity resonant frequency. The laser wavelength is $\lambda = 1064$ nm, the optical lengths are $l_1 = l_2 = l_{a1} = l_{a2} = 28.196$ mm, the reflectivity of the four end mirrors are $r_0^2 = 0.986$, $r_2^2 = 0.9$ and $r_{a1}^2 = r_{a2}^2 = 1$. (a) $\theta_{a1} = 2n\pi + \omega T + 0.0005\pi$ and $\theta_{a2} = 2n\pi + \omega T - 0.0005\pi$. (b) $\theta_{a1} = 2n\pi + \omega T + 0.003\pi$ and $\theta_{a2} = 2n\pi + \omega T - 0.003\pi$. (c) $\theta_{a1} = 2n\pi + \omega T + 0.007\pi$ and $\theta_{a2} = 2n\pi + \omega T - 0.007\pi$. (d) $\theta_{a1} = 2n\pi + \omega T + 0.01\pi$ and $\theta_{a2} = 2n\pi + \omega T - 0.01\pi$. (e) $\theta_{a1} = 2n\pi + \omega T + 0.04\pi$ and $\theta_{a2} = 2n\pi + \omega T - 0.04\pi$. (f) $\theta_{a1} = 2n\pi + \omega T + 0.06\pi$ and $\theta_{a2} = 2n\pi + \omega T - 0.06\pi$.

3. Quantum characteristic of DRMI

In quantum optics, a quantum state is described by amplitude quadrature $\hat{X} = (\hat{a} + \hat{a}^\dagger)$ and phase quadrature $\hat{Y} = -i(\hat{a} - \hat{a}^\dagger)$ with the canonical commutation relation $[\hat{X}, \hat{Y}] = 2i$, where \hat{a} and \hat{a}^\dagger are the photon annihilation operator and creation operator. Since the quantum fluctuation of quantum state is usually measured and analyzed in frequency domain, the Fourier transformation $\frac{1}{\sqrt{2\pi}} \int dt \hat{a}(t) e^{-i\omega t}$ is implemented for the amplitude and phase quadratures

$$\begin{aligned}\hat{X}_{out}(\omega) &= \hat{a}_{out}(\omega) + \hat{a}_{out}^\dagger(-\omega) \\ \hat{Y}_{out}(\omega) &= -i \left[\hat{a}_{out}(\omega) - \hat{a}_{out}^\dagger(-\omega) \right]\end{aligned}\quad (4)$$

According to the reflected coefficient γ_2 of dual-recycled Michelson interferometer, the reflective quantum field in frequency domain is

$$\begin{aligned}\hat{a}_{out}(\omega) &= \rho(\omega_0 + \omega) e^{i\theta(\omega_0 + \omega)} \hat{a}_{in}(\omega) + \sqrt{1 - \rho^2(\omega_0 + \omega)} \hat{a}_v(\omega) \\ \hat{a}_{out}^\dagger(-\omega) &= \rho(\omega_0 - \omega) e^{-i\theta(\omega_0 - \omega)} \hat{a}_{in}^\dagger(-\omega) + \sqrt{1 - \rho^2(\omega_0 - \omega)} \hat{a}_v^\dagger(-\omega)\end{aligned}\quad (5)$$

where ω_0 and ω are the central frequency and analysis frequency respectively, \hat{a}_v is the vacuum field introduced by optical loss. The input bright field can be expressed as $\hat{a}_{in} = a_{in} + \delta\hat{a}_{in}$, in which a_{in} is the mean field and $\delta\hat{a}_{in}$ is the quantum fluctuation. Considering only the quantum

field ($a_{in} = 0$), we can acquire the fluctuation variances of the amplitude and phase quadratures

$$\begin{aligned} \langle \delta^2 X_{out}(\omega) \rangle &= \frac{1}{4} \left| \rho(\omega_0 + \omega) e^{i\theta(\omega_0 + \omega)} + \rho(\omega_0 - \omega) e^{-i\theta(\omega_0 - \omega)} \right|^2 \langle \delta^2 X_{in}(\omega) \rangle \\ &+ \frac{1}{4} \left| \rho(\omega_0 + \omega) e^{i\theta(\omega_0 + \omega)} - \rho(\omega_0 - \omega) e^{-i\theta(\omega_0 - \omega)} \right|^2 \langle \delta^2 Y_{in}(\omega) \rangle \\ &+ \frac{1}{4} \left| \sqrt{1 - \rho^2(\omega_0 + \omega)} + \sqrt{1 - \rho^2(\omega_0 - \omega)} \right|^2 \langle \delta^2 X_v(\omega) \rangle \\ &+ \frac{1}{4} \left| \sqrt{1 - \rho^2(\omega_0 + \omega)} - \sqrt{1 - \rho^2(\omega_0 - \omega)} \right|^2 \langle \delta^2 Y_v(\omega) \rangle \end{aligned} \quad (6)$$

$$\begin{aligned} \langle \delta^2 Y_{out}(\omega) \rangle &= \frac{1}{4} \left| -\rho(\omega_0 + \omega) e^{i\theta(\omega_0 + \omega)} + \rho(\omega_0 - \omega) e^{-i\theta(\omega_0 - \omega)} \right|^2 \langle \delta^2 X_{in}(\omega) \rangle \\ &+ \frac{1}{4} \left| \rho(\omega_0 + \omega) e^{i\theta(\omega_0 + \omega)} + \rho(\omega_0 - \omega) e^{-i\theta(\omega_0 - \omega)} \right|^2 \langle \delta^2 Y_{in}(\omega) \rangle \\ &+ \frac{1}{4} \left| -\sqrt{1 - \rho^2(\omega_0 + \omega)} + \sqrt{1 - \rho^2(\omega_0 - \omega)} \right|^2 \langle \delta^2 X_v(\omega) \rangle \\ &+ \frac{1}{4} \left| \sqrt{1 - \rho^2(\omega_0 + \omega)} + \sqrt{1 - \rho^2(\omega_0 - \omega)} \right|^2 \langle \delta^2 Y_v(\omega) \rangle \end{aligned} \quad (7)$$

Here the fluctuation variances of the vacuum field are normalized so that $\langle \delta^2 X_v(\omega) \rangle = \langle \delta^2 Y_v(\omega) \rangle = 1$. When the input state \hat{a}_{in} is a vacuum (coherent) state, the reflected state of DRMI will also be a vacuum (coherent) state with normalized fluctuation variances for both quadratures. When the input state \hat{a}_{in} is a pure squeezed vacuum state, whose fluctuation variance of the amplitude and phase quadratures can be written as $\langle \delta^2 X_{in}(\omega) \rangle = e^{2s}$ and $\langle \delta^2 Y_{in}(\omega) \rangle = e^{-2s}$, the reflective quantum fluctuation near resonance will be affected by the absorption and dispersion characteristics of dual-recycled Michelson interferometer. For different relative phase between two interference arms $\theta_{a1} - \theta_{a2} = 0.001\pi, 0.006\pi, 0.014\pi, 0.02\pi, 0.08\pi$, and 0.12π , the fluctuation variances of the amplitude and phase quadratures as function of detuning frequency are shown in Fig. 3(a)-(f). The input squeezing level in Fig. 3 is chosen to be 15 dB below the shot noise limit, which is the world record for current experimental squeezed state generation. The blue curves depict the reflected amplitude quadrature spectrum, while red curves represent the reflected phase quadrature spectra.

In Fig. 3(a), the line shape of the quantum fluctuation variance of phase quadrature for the reflective field exhibits M profile, in which two peaks at detuning frequencies reach the anti-squeezing level of input squeezed vacuum, caused by the phase shift $\pm\pi/2$ of DRMI. The squeezing level at resonant frequency ω_0 (zero detuning) is below the shot noise limit and will reach the input squeezing level for perfect impedance matching. When the detuning frequency is far away from resonant frequency, the absorption and dispersion characteristics will not affect the fluctuation variance of input state. Corresponding, the line shape of the quantum fluctuation variance of amplitude quadrature represents W profile, and two dips at detuning frequencies show the initial squeezing level 15 dB. Therefore, the squeezing angles of the reflective field are rotating with different detuning frequency, which is equivalent to the phase sensitive manipulation of squeezed vacuum state by single optical cavity.

When the coupling strength Ω is about $2\pi * 8.0$ MHz, the dip around resonant frequency will split into two dips (red curve in Fig. 3(b)) because of the coupled-resonator-induced transparent window shown in Fig. 2(b). The fluctuation variance of phase quadrature in the near resonant region exhibits three peaks and two dips in total, while the fluctuation variance of amplitude quadrature represents two peaks and three dips. Increasing the coupling strength to $2\pi * 18.6$ MHz, the quantum spectra will continue to split (Fig. 3(c)), and the fluctuation variance of phase

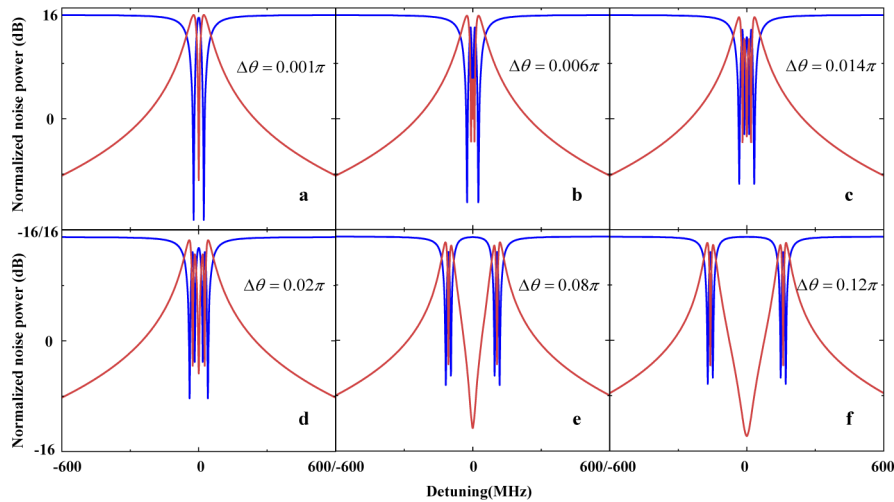


Fig. 3. Theoretical results of the reflective quantum fluctuation spectra of dual-recycled Michelson interferometer for different coupling strength. The blue curves in (a)-(f) are the reflected amplitude quadrature spectrum, while red curves represent the reflected phase quadrature spectra. The reflectivity of four end mirrors and single-pass phases (θ_0 and θ_2) are identical with Fig. 2. The single-pass phases θ_{a1} and θ_{a2} in Fig. 3(a)-(f) are one-to-one corresponding to that in Fig. 2(a)-(f). The input squeezed vacuum state is 15 dB below the shot noise limit.

(amplitude) quadrature will show four (three) peaks and three (four) dips. Due to the increased width of coupled-resonator-induced transparent window, the detuning frequencies where peaks and dips appear will augment with the increasing coupling strength (Fig. 3(d)-(e)).

Continuing to increase the coupling strength, the fluctuation variances for both quadratures will separate into two sets of spectra (Fig. 3(f)), similar to the phenomena of two independent optical cavity. It needs to be emphasized that the detuning frequencies of peaks and dips in Fig. 3 are one-to-one correspondent to the absorption and dispersion characteristics in Fig. 2. Thus the phase sensitive manipulation of vacuum squeezed state is achieved by coupled-resonator-induced transparency effect in dual-recycled Michelson interferometer.

Furthermore, the corner point from anti-squeezing to squeezing can be tuned by the relative phase difference $\Delta\theta$ between two interference arms θ_{a1} and θ_{a2} , as depicted in Fig. 4. The corner point can be utilized to generate the so-called frequency dependent squeezing that can provide broadband quantum noise reduction for gravitational wave detectors. Thus the rotation frequency of squeezing ellipse can be finely tuned by the relative phase difference $\Delta\theta$, which is difficult to adjust in traditional scheme for frequency dependent squeezing generation.

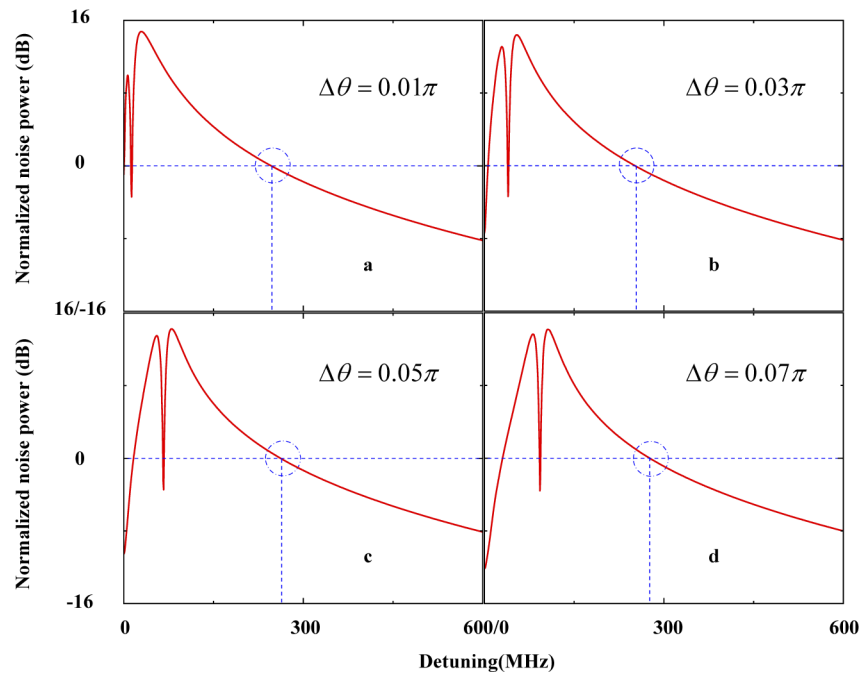


Fig. 4. Transition point from anti-squeezing to squeezing with different phase difference $\Delta\theta$. (a) $\Delta\theta = 0.01\pi$. (b) $\Delta\theta = 0.03\pi$. (c) $\Delta\theta = 0.05\pi$. (d) $\Delta\theta = 0.07\pi$.

4. Conclusion

In conclusion, we have proposed the phase sensitive manipulation scheme of squeezed vacuum state via dual-recycled Michelson interferometer (DRMI). By simulating the injection of the squeezed vacuum state into DRMI, we attentively analyze the fluctuation variances for amplitude quadrature and phase quadrature of reflected field. The quantum spectra are one-to-one correspondent to the coupled-resonator-induced transparency effect of DRMI, whose coupling strength can be controlled fleetly by adjusting the relative phase difference of interferometer arms. Moreover, the rotation frequency of frequency-dependent squeezing can be finely tuned by the coupling strength. This work has broad prospect applications in quantum memory and quantum metrology including GWD, etc.

Funding. National Natural Science Foundation of China (62027821, 11654002, 62035015, 11804206, 61805133); National Key Research and Development Program of China (2020YFC2200402); Scientific and Technological Innovation Programs of Higher Education Institutions in Shanxi (2020L0015); Key R&D Projects of Shanxi (201903D111001); Program for Sanjin Scholar of Shanxi Province; Fund for Shanxi “1331 Project” Key Subjects Construction.

Disclosures. The authors declare no conflicts of interest.

Data availability. Data underlying the results presented in this paper are not publicly available at this time but may be obtained from the authors upon reasonable request.

References

1. LIGO Scientific Collaboration and Virgo Collaboration, “Observation of gravitational waves from a binary black hole merger,” *Phys. Rev. Lett.* **116**(6), 061102 (2016).
2. S. Vitale, “The first 5 years of gravitational-wave astrophysics,” *Science* **372**(6546), eabc7397 (2021).
3. LIGO Scientific Collaboration and Virgo Collaboration, “GW151226: Observation of gravitational waves from a 22-solar-mass binary black hole coalescence,” *Phys. Rev. Lett.* **116**(24), 241103 (2016).
4. LIGO Scientific Collaboration and Virgo Collaboration, “GWTC-2: compact binary coalescences observed by LIGO and Virgo during the first half of the third observing run,” *Phys. Rev. X* **11**(2), 021053 (2021).

5. T. Venumadhav, B. Zackay, J. Roulet, L. Dai, and M. Zaldarriaga, “New binary black hole mergers in the second observing run of Advanced LIGO and Advanced Virgo,” *Phys. Rev. D* **101**(8), 083030 (2020).
6. B. Zackay, T. Venumadhav, L. Dai, J. Roulet, and M. Zaldarriaga, “Highly spinning and aligned binary black hole merger in the Advanced LIGO first observing run,” *Phys. Rev. D* **100**(2), 023007 (2019).
7. The L. I. G. O. Scientific Collaboration and the Virgo Collaboration, “GW170817: measurements of neutron star radii and equation of state,” *Phys. Rev. Lett.* **121**(16), 161101 (2018).
8. The L. I. G. O. Scientific Collaboration, the Virgo Collaboration and the K. A. G. R. A. C. Collaboration, “Observation of Gravitational waves from two neutron star-black hole coalescences,” *The Astrophys. J. Lett.* **915**(1), L5 (2021).
9. LIGO Scientific Collaboration and Virgo Collaboration, “GW150914: the advanced LIGO detectors in the era of first discoveries,” *Phys. Rev. Lett.* **116**(13), 131103 (2016).
10. LIGO Scientific Collaboration and Virgo Collaboration, “GW170817: observation of gravitational waves from a binary neutron star inspiral,” *Phys. Rev. Lett.* **119**(16), 161101 (2017).
11. LIGO Scientific and Virgo Collaboration, “GW170104: observation of a 50-solar-mass binary black hole coalescence at redshift 0.2,” *Phys. Rev. Lett.* **118**(22), 221101 (2017).
12. H. Miao, H. Yang, R. X. Adhikari, and Y. Chen, “Quantum limits of interferometer topologies for gravitational radiation detection,” *Classical Quantum Gravity* **31**(16), 165010 (2014).
13. M. Punturo, M. Punturo, M. Abernathy, F. Acernese, B. Allen, N. Andersson, K. Arun, F. Barone, B. Barr, M. Barsuglia, M. Beker, N. Beveridge, S. Birindelli, S. Bose, L. Bosi, S. Braccini, C. Bradaschia, T. Bulik, E. Calloni, G. Cella, E. Chassande Mottin, S. Chelkowsky, A. Chincarini, J. Clark, E. Coccia, C. Colacino, J. Colas, A. Cumming, L. Cunningham, E. Cuoco, S. Danilishin, K. Danzmann, G. De Luca, R. De Salvo, T. Dent, R. Derosa, L. Di Fiore, A. Di Virgilio, M. Doets, V. Fafone, P. Falferi, R. Flaminio, J. Franc, F. Frasconi, A. Freise, P. Fulda, J. Gair, G. Gemme, A. Gennai, A. Giazotto, K. Glampedakis, M. Granata, H. Grote, G. Guidi, G. Hammond, M. Hannam, J. Harms, D. Heinert, M. Hendry, I. Heng, E. Hennes, S. Hild, J. Hough, S. Husa, S. Huttner, G. Jones, F. Khalili, K. Kokeyama, K. Kokkotas, B. Krishnan, M. Lorenzini, H. Luck, E. Majorana, I. Mandel, V. Mandic, I. Martin, C. Michel, Y. Minenkov, N. Morgado, S. Mosca, B. Mours, H. Müller-Ebhardt, P. Murray, R. Nawrodt, J. Nelson, R. Oshaughnessy, C. D. Ott, C. Palomba, A. Paoli, G. Parguez, A. Pasqualetti, R. Passaquieti, D. Passuello, L. Pınard, R. Poggiani, P. Popolizio, M. Prato, P. Puppo, D. Rabeling, P. Rapagnani, J. Read, T. Regimbau, H. Rehbein, S. Reid, L. Rezzolla, F. Ricci, F. Richard, A. Rocchi, S. Rowan, A. Rüdiger, B. Sassolas, B. Sathyaprakash, R. Schnabel, C. Schwarz, P. Seidel, A. Sintes, K. Somiya, F. Speirits, K. Strain, S. Strigin, P. Sutton, S. Tarabrin, J. van den Brand, C. van Leewen, M. van Veggel, C. van den Broeck, A. Vecchio, J. Veitch, F. Vettrano, A. Vicere, S. Vyatchanin, B. Willke, G. Woan, P. Wolfango, and K. Yamamoto, “The third generation of gravitational wave observatories and their science reach,” *Classical Quantum Gravity* **27**(8), 084007 (2010).
14. R. E. Slusher, L. W. Hollberg, B. Yurke, J. C. Mertz, and J. F. Valley, “Observation of squeezed states generated by four-wave mixing in an optical cavity,” *Phys. Rev. Lett.* **55**(22), 2409–2412 (1985).
15. Q. Wang, Y. Tian, W. Li, L. Tian, Y. Wang, and Y. Zheng, “High-fidelity quantum teleportation toward cubic phase gates beyond the no-cloning limit,” *Phys. Rev. A* **103**(6), 062421 (2021).
16. N. Wang, S. Du, W. Liu, X. Wang, Y. Li, and K. Peng, “Long-distance continuous-variable quantum key distribution with entangled states,” *Phys. Rev. Appl.* **10**(6), 064028 (2018).
17. S. Shi, L. Tian, Y. Wang, Y. Zheng, C. Xie, and K. Peng, “Demonstration of channel multiplexing quantum communication exploiting entangled sideband modes,” *Phys. Rev. Lett.* **125**(7), 070502 (2020).
18. Y. Xia, W. Li, W. Clark, D. Hart, Q. Zhuang, and Z. Zhang, “Demonstration of a reconfigurable entangled radio-frequency photonic sensor network,” *Phys. Rev. Lett.* **124**(15), 150502 (2020).
19. C. M. Caves, “Quantum-mechanical noise in an interferometer,” *Phys. Rev. D* **23**(8), 1693–1708 (1981).
20. H. Vahlbruch, S. Chelkowsky, B. Hage, A. Franzen, K. Danzmann, and R. Schnabel, “Demonstration of a squeezed-light-enhanced power- and signal-recycled Michelson interferometer,” *Phys. Rev. Lett.* **95**(21), 211102 (2005).
21. K. Goda, O. Miyakawa, E. E. Mikhailov, S. Saraf, R. Adhikari, K. McKenzie, R. Ward, S. Vass, A. J. Weinstein, and N. Mavalvala, “A quantum-enhanced prototype gravitational-wave detector,” *Nat. Phys.* **4**(6), 472–476 (2008).
22. The L. I. G. O. Scientific Collaboration, “A gravitational wave observatory operating beyond the quantum shot-noise limit,” *Nat. Phys.* **7**(12), 962–965 (2011).
23. The L. I. G. O. Scientific Collaboration, “Enhanced sensitivity of the LIGO gravitational wave detector by using squeezed states of light,” *Nat. Photonics* **7**(8), 613–619 (2013).
24. M. Tse, H. Yu, N. Kijbunchoo, A. Fernandez-Galiana, P. Dupej, L. Barsotti, C. D. Blair, D. D. Brown, S. E. Dwyer, A. Effler, M. Evans, P. Fritschel, V. V. Frolov, A. C. Green, G. L. Mansell, F. Matichard, N. Mavalvala, D. E. McClelland, L. McCuller, T. McRae, J. Miller, A. Mullavey, E. Oelker, I. Y. Phinney, D. Sigg, B. J. J. Slagmolen, T. Vo, R. L. Ward, C. Whittle, R. Abbott, C. Adams, R. X. Adhikari, A. Ananyeva, S. Appert, K. Arai, J. S. Areeda, Y. Asali, S. M. Aston, C. Austin, A. M. Baer, M. Ball, S. W. Ballmer, S. Banagiri, D. Barker, J. Bartlett, B. K. Berger, J. Betzwieser, D. Bhattacharjee, G. Billingsley, S. Biscans, R. M. Blair, N. Bode, P. Booker, R. Bork, A. Bramley, A. F. Brooks, A. Buikema, C. Cahillane, K. C. Cannon, X. Chen, A. A. Ciobanu, F. Clara, S. J. Cooper, K. R. Corley, S. T. Countryman, P. B. Covas, D. C. Coyne, L. E. H. Datrier, D. Davis, C. DiFronzo, J. C. Driggers, T. Etzel, T. M. Evans, J. Feicht, P. Fulda, M. Fyffe, J. A. Giaime, K. D. Giardina, P. Godwin, E. Goetz, S. Gras, C. Gray, R. Gray, A. Gupta, E. K. Gustafson, R. Gustafson, J. Hanks, J. Hanson, T. Hardwick, R. K. Hasskew, M. C. Heintze, A. F. Helmling-Cornell, N. A. Holland, J. D. Jones, S. Kandhasamy, S. Karki, M. Kasprzack, K. Kawabe, P. J. King, J. S. Kissel, R. Kumar, M. Landry, B. B. Lane, B. Lantz, M. Laxen, Y. K. Lecoeuche, J. Leviton, J. Liu, M. Lormand,

- A. P. Lundgren, R. Macas, M. MacInnis, D. M. Macleod, S. Márka, Z. Márka, D. V. Martynov, K. Mason, T. J. Massinger, R. McCarthy, S. McCormick, J. McIver, G. Mendell, K. Merfeld, E. L. Merilh, F. Meylahn, T. Mistry, R. Mittleman, G. Moreno, C. M. Mow-Lowry, S. Mozzon, T. J. N. Nelson, P. Nguyen, L. K. Nuttall, J. Oberling, R. J. Oram, B. O'Reilly, C. Osthelder, D. J. Ottaway, H. Overmier, J. R. Palamos, W. Parker, E. Payne, A. Pele, C. J. Perez, M. Pirello, H. Radkins, K. E. Ramirez, J. W. Richardson, K. Riles, N. A. Robertson, J. G. Rollins, C. L. Romel, J. H. Romie, M. P. Ross, K. Ryan, T. Sadecki, E. J. Sanchez, L. E. Sanchez, T. R. Saravanan, R. L. Savage, D. Schaeztl, R. Schnabel, R. M. S. Schofield, E. Schwartz, D. Sellers, T. J. Shaffer, J. R. Smith, S. Soni, B. Sorazu, A. P. Spencer, K. A. Strain, L. Sun, M. J. Szczepańczyk, M. Thomas, P. Thomas, K. A. Thorne, K. Toland, C. I. Torrie, G. Traylor, A. L. Urban, G. Vajente, G. Valdes, D. C. Vander-Hyde, P. J. Veitch, K. Venkateswara, G. Venugopalan, A. D. Viets, C. Vorvick, M. Wade, J. Warner, B. Weaver, R. Weiss, B. Willke, C. C. Wipf, L. Xiao, H. Yamamoto, M. J. Yap, H. Yu, L. Zhang, M. E. Zucker, and J. Zweizig, "Quantum-enhanced advanced LIGO detectors in the era of gravitational-wave astronomy," *Phys. Rev. Lett.* **123**(23), 231107 (2019).
25. E. Capocasa, M. Barsuglia, J. Degallaix, L. Pinard, N. Straniero, R. Schnabel, K. Somiya, Y. Aso, D. Tatsumi, and R. Flaminio, "Estimation of losses in a 300 m filter cavity and quantum noise reduction in the KAGRA gravitational-wave detector," *Phys. Rev. D* **93**(8), 082004 (2016).
26. J. Südbeck, S. Steinlechner, M. Korobko, and R. Schnabel, "Demonstration of interferometer enhancement through Einstein–Podolsky–Rosen entanglement," *Nat. Photonics* **14**(4), 240–244 (2020).
27. M. Evans, L. Barsotti, and P. Kwee, "Realistic filter cavities for advanced gravitational wave detectors," *Phys. Rev. D* **88**(2), 022002 (2013).
28. J. Qin, C. Zhao, Y. Ma, X. Chen, L. Ju, and B. G. David, "Classical demonstration of frequency-dependent noise ellipse rotation using optomechanically induced transparency," *Phys. Rev. A* **89**(4), 041802 (2014).
29. H. J. Kimble, Y. Levin, A. B. Matsko, K. S. Thorne, and S. P. Vyatchanin, "Conversion of conventional gravitational-wave interferometers into quantum nondemolition interferometers by modifying their input and/or output optics," *Phys. Rev. D* **65**(2), 022002 (2001).
30. S. Chelkowski, H. Vahlbruch, B. Hage, A. Franzen, N. Lastzka, K. Danzmann, and R. Schnabel, "Experimental characterization of frequency-dependent squeezed light," *Phys. Rev. A* **71**(1), 013806 (2005).
31. E. Oelker, T. Isogai, J. Miller, M. Tse, L. Barsotti, N. Mavalvala, and M. Evans, "Audio-band frequency-dependent squeezing for gravitational-wave detectors," *Phys. Rev. Lett.* **116**(4), 041102 (2016).
32. L. McCuller, C. Whittle, D. Ganapathy, K. Komori, M. Tse, A. Fernandez-Galiana, L. Barsotti, P. Fritschel, M. MacInnis, F. Matichard, K. Mason, N. Mavalvala, R. Mittleman, and H. Yu, "Frequency-dependent squeezing for advanced LIGO," *Phys. Rev. Lett.* **124**(17), 171102 (2020).
33. Y. Zhao, N. Aritomi, E. Capocasa, M. Leonardi, M. Eisenmann, Y. Guo, E. Polini, A. Tomura, K. Arai, Y. Aso, Y. Huang, R. Lee, H. Lück, O. Miyakawa, P. Prat, A. Shoda, M. Tacca, R. Takahashi, H. Vahlbruch, M. Vardaro, C. Wu, M. Barsuglia, and R. Flaminio, "Frequency-dependent squeezed vacuum source for broadband quantum noise reduction in advanced gravitational-wave detectors," *Phys. Rev. Lett.* **124**(17), 171101 (2020).
34. K. Di, C. Xie, and J. Zhang, "Coupled-resonator-induced transparency with a squeezed vacuum," *Phys. Rev. Lett.* **106**(15), 153602 (2011).
35. X. Yu, W. Li, Y. Jin, and J. Zhang, "Controllable coupled-resonator-induced transparency in a dual-recycled Michelson interferometer," *Phys. Rev. A* **98**(5), 053854 (2018).